JOURNAL OF MATERIALS SCIENCE **38** (2003) 471–480

Strength of thermally exposed alumina fibers

Part II *bundle behavior*

P. E. CANTONWINE*
Materials Science and Engineering Department, University of Virginia, Charlottesville, VA 22903, USA

Non-ideal bundle models that predict the effect of filament slack, misalignment and bonding were compared to the predicted ideal bundle stress-strain response and the measured response of an Alumina tow (Nextel™ 610) as a function of exposure temperature. The ideal bundle model assumes that the filaments are perfectly aligned, independent, and filament strength is characterized by single filament tests; the non-ideal bundle models relax these assumptions. The Nextel™ 610 tow was found to behave ideally until the sintering bonds between filaments were strong enough to resist fracture during testing. When bonded filament clusters existed throughout testing, the weakest filament in the cluster likely caused failure of the entire cluster. Therefore, the assumption of independence was not valid, and the measured bundle strength was lower than the ideal bundle prediction. The assumption that the strength distribution of the bonded filaments was the same as the filaments removed from bonded filament clusters also appears to be invalid. It is hypothesized that the effective decrease in strength of bonded filaments is a result of induced shear stresses that form along the bond line when bonded filaments are either bent or twisted. However, within a composite this motion is limited. The modeling indicated that 10% clustering can be tolerated with little degradation in composite properties as long as the clusters remain independent from their neighbors.
© *2003 Kluwer Academic Publishers*

1. Introduction

Continuous reinforced composites are bundles of filaments "glued" together with a metal, ceramic or polymer matrix. Thus, it is not surprising that the models developed to predict the stress-strain response of these composites are based on the behavior of filament bundles [1, 2]. Filament bundles have long been a concern in the textile industry [3, 4], and the ideal bundle model developed by Daniels [5], which allowed for the accumulation of filament failures, ultimately explained why the strength of a bundle was significantly less that the average strength of the constituent filaments. In the late 1950s, Coleman [6] applied Daniels' model to weakest-link filaments whose strengths followed a Weibull distribution. This allowed the model to be applied to advance composite materials where the reinforcements were stiff, strong and brittle [1, 2]. Three important assumptions of the ideal bundle model are that the filaments are perfectly aligned in the loading direction, filament failure occurs independent of neighboring filaments, and load from a failed filament is evenly distributed among the remaining unbroken filaments (global load sharing).

Continuous oxide reinforcements are most economically manufactured as multifilament tows or bundles. Typically the process involves spinning hundreds to thousands of filaments from a liquid organic precursor followed by solidifying, drying, and firing. An example of such a multifilament tow is the Nextel™ 610 fiber, a small-grain Al_2O_3 filament manufactured by 3M (see Fig. 1); Nextel™ 610 has been used to reinforce various materials from titanium alloys [7, 8] to ceramics [9], but it is apparent from Fig. 1 that the filaments are not perfectly aligned.

Two types of alignment defects occur naturally in multifilament tows: filament slack and filament misalignment. Filament slack is caused by variations in filament length over a given length of tow and results in the shorter filaments being loaded before the longer filaments (i.e., there is a distribution in filament strains). It will be assumed herein that when loaded these "slacked" filaments are perfectly aligned. Filament misalignment refers to filaments that are oriented at an angle to the loading direction also causing a distribution in filament strains.[1] A third type of defect, which is not apparent in Fig. 1, results from filament-to-filament sintering after high temperature exposure.

In Part I [10] the single filament strength distribution of Nextel™ 610 was determined as a function

[1] It is recognized that a filament slack defect likely will turn into a filament misalignment defect once the filament is loaded but this will not modeled.

Present Address: Bechtel Bettis Inc., P.O. Box 79, ZAP 14B, West Mifflin, PA 15122, USA.

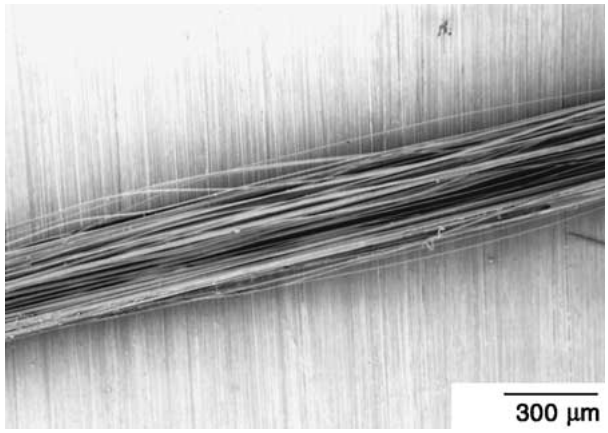

Figure 1 As-received Nextel™ 610 tow fiber with the polymer sizing removed.

of thermal exposure; filament strength was found to decrease as exposure temperature increased. The measured strength distribution characterizes the independent failure of filaments within the bundle (an assumption in the ideal bundle model). Thus, the results from Part I were used with the ideal bundle model to define a hypothesized stress-strain response for Nextel™ 610 bundles. The two main objectives of this work were (1) to measure the stress-strain response of Nextel™ 610 bundles as a function of thermal exposure and to compare that response to the ideal bundle model, and (2) to develop "non-ideal" models that predict the effect of filament slack, filament misalignment, and filament-to-filament sintering. By comparing the non-ideal model results to the measurements, the relative importance of each bundle defect can be determined. Another objective was to characterize the evolution of the defect distribution with exposure temperature and compare it to previous results reported in Part I [10].

2. The ideal bundle model

An ideal filament bundle is a collection of a "large" number (greater than 200 [11]) of independent filaments oriented in a parallel array. When stress is applied to the bundle, it is assumed to be evenly distributed to all the filaments. At a stress much lower then the mean filament strength, the first filament fails. This filament becomes completely ineffective, and the load it once carried is then assumed to be evenly redistributed over the remaining filaments. This concept is called global load sharing.

The bundle stress, σ_b, is defined as the load divided by the initial area of all the filaments. The bundle stress will be equivalent to the filament stress until filaments begin to fail. At that point the single filament stress become larger than the bundle stress. As defined by Daniels [5] and Coleman [6], the ideal bundle stress is:

$$\sigma_b = \sigma_f(1 - P_f) \tag{1}$$

where σ_f is the applied stress in an unbroken filament and P_f is the probability of failure, which can be determined from the Weibull distribution:

$$P_f = 1 - \exp\left(-\frac{L}{L_o}\left(\frac{\sigma_f}{\sigma_o}\right)^m\right) \tag{2}$$

where L is the gauge length and L_o, σ_o and m are the Weibull parameters determined from single filament tests. The probability of failure is equivalent to the fraction of filaments that have failed in a bundle. Equation 1 is therefore a simple rule of mixtures model.

By substituting Equation 2 into Equation 1 and using Hooke's law for the filament stress, the bundle stress can be written as a function of strain, ε.

$$\sigma_b = E_f\,\varepsilon \exp\left(-\frac{L}{L_o}\left(\frac{E_f\,\varepsilon}{\sigma_o}\right)^m\right) \tag{3}$$

The failure strain of the bundle, $\varepsilon_{\text{fail}}$, is found by differentiating Equation 3 with respect to strain, setting it equal to zero, and solving for the strain:

$$\varepsilon_{\text{fail}} = \frac{\sigma_o}{E_f}\left(\frac{Lm}{L_o}\right)^{-1/m} \tag{4}$$

The bundle strength, σ_b^*, is found by substituting Equation 4 into Equation 3 to give:

$$\sigma_b^* = \sigma_{\text{fail}} \exp\left(-\frac{1}{m}\right) \tag{5}$$

recognizing that $\sigma_{\text{fail}} = E_f\,\varepsilon_{\text{fail}}$,

3. Experimental procedures

3.1. Materials and processing

Nextel™ 610 is 99.5% Al_2O_3. For a denier of 1500, there are approximately 400 filaments per tow; the filament diameter is approximately 12 μm [12]. The filaments are manufactured from an organic basic aluminum salt solution. The "green" filaments are spun from a multi-orifice spinnerette, fired slowly to remove the volatiles and then converted to alpha alumina at 1400°C [12]. The Nextel™ 610 fiber tow is a high strength reinforcement used in metal and ceramic matrices [13]. The high strength is achieved by keeping the grain size small (less than 100 nm) and minimizing the process induced defects [13].

The effects of thermal exposure were investigated via a continuous heat-treatment process. The Nextel™ 610 was continuously drawn at 30 cm/min. through two furnaces; the line tension was around 0.7 N to avoid significant sagging. To burn off residual organics such as the sizing, the temperature of the first furnace was set at 750°C. The second (or sintering) furnace was set at temperatures ranging from 1100 to 1450°C. Since the hot zone was about 30 cm in length, the filaments were at temperature for about 1 minute. To investigate the possible introduction of handling flaws, an experiment to represent the as-received condition was done with the sintering furnace at room temperature. The final step was to resize the bundle by infiltrating it with a polyvinyl butyral/methanol solution followed by curing. The resizing step allowed for more uniform griping of the filaments during the testing of the filament bundles. This continuous process for sample preparation was developed, in part, to minimized the possibility of increasing the number of filament-slack and filament-misalignment defects in the bundle test specimens.

3.2. Testing

Sized filament bundles (∼13 cm in length) were put into a 2.5 cm long furnace to burn-off the organic sizing within the approximate 2.5 cm gauge length, which eliminated the ability of neighboring filaments to communicate through shear stresses in the sizing. The bundles were then mounted into paper tabs. The stress-strain response of the bundles was measured at room temperature using an ATS series 1100 tensile testing machine with a 50 lb. load cell, 0.25 cm/min crosshead speed, rubber face grips and an OPTRA 3000 laser extensometer. Selected bundles were infiltrated with petroleum jelly to dampen the shock waves during failure, thus saving the fracture surfaces for fractography.

4. Alumina filament bundle behavior

The stress-strain responses after four different heat treatments are plotted in Fig. 2. The measured bundle strength is plotted versus exposure temperature in Fig. 3. The predicted response of an ideal bundle is shown in these figures for comparison; the measured Weibull parameters for each exposure were reported in Part I [10] and are reproduced in Table I. The bundles in the as-received condition and exposed to 1300°C were well predicted by the ideal bundle model. The model overpredicts the measured modulus and bundle strength by less than 10%. In contrast, for exposures above 1300°C, the ideal bundle model overpredicts the

TABLE I Filament strength parameters

Exposure temperature	Weibull reference stress (GPa)	Weibull modulus
As-received	3.37	11.0
1100°C	3.30	7.1
1200°C	3.30	7.0
1300°C	3.09	7.0
1350°C	3.10	8.1
1400°C	3.00	9.0
1450°C	2.51	11.0

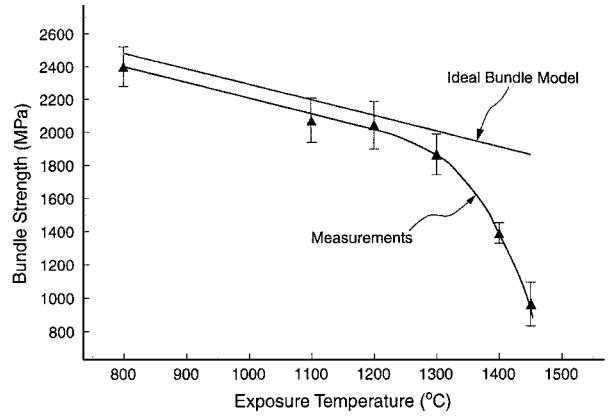

Figure 3 Bundle strength of Nextel™ 610 versus exposure temperature. The bundles exposed at 800°C where considered to represent the as-received condition.

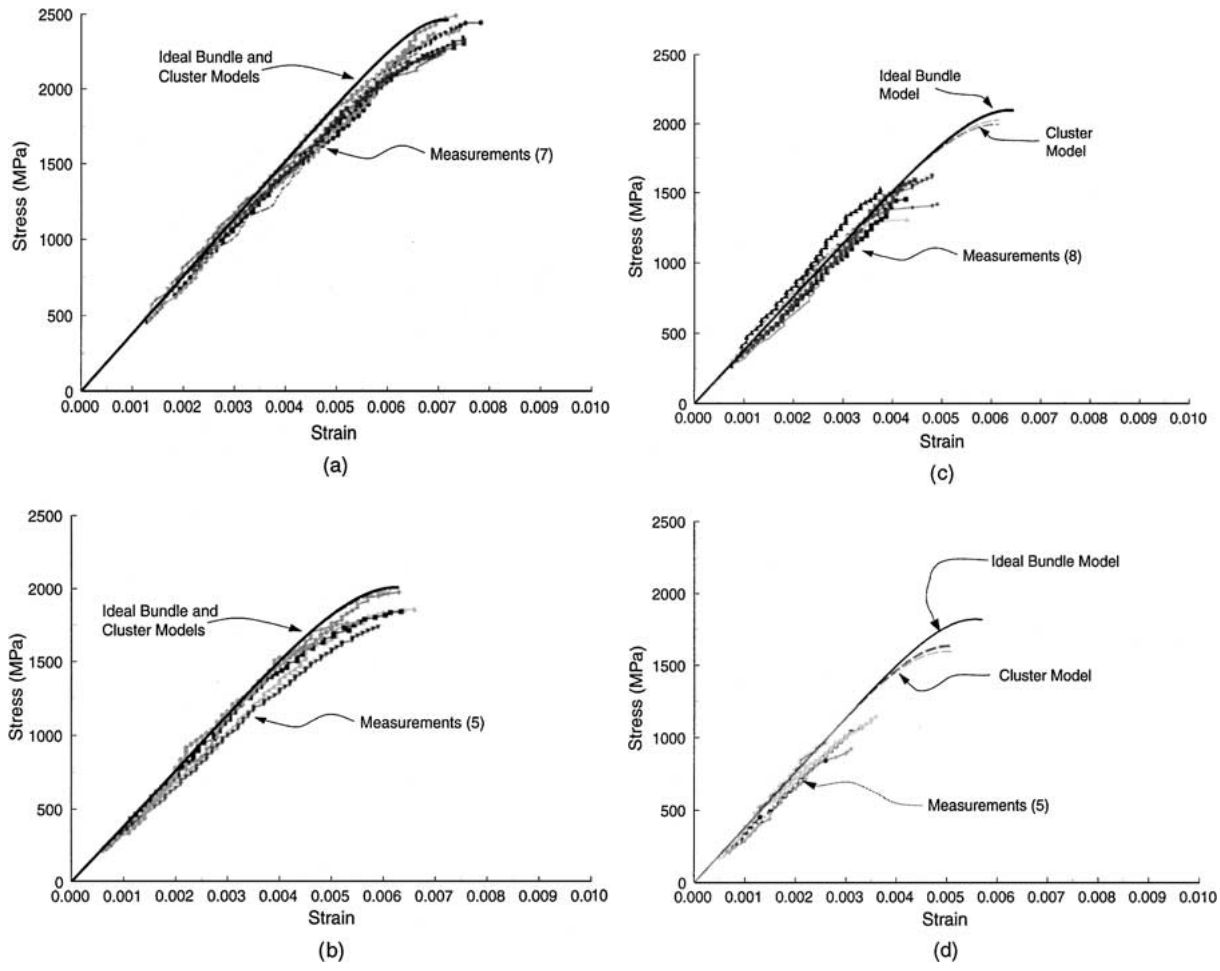

Figure 2 Stress-Strain measurements, ideal bundle predictions and non-ideal cluster predictions (Section 5.3) for (a) as-received alumina bundles, (b) exposed at 1300°C, (c) exposed at 1400°C and (d) exposed at 1450°C.

TABLE II Defect distribution; bundle tests

Exposure temperature	Defect type							
	SU[1]	SW[2]	SC[3]	SN[4]	SB[5]	IU[6]	IP[7]	IPY[8]
As-received	32%	4%	4%	7%	—	21%	23%	9%
1300°C	25%	25%	2%	6%	6%	17%	15%	4%
1400°C	30%	68%	—	—	—	—	2%	—
1450°C	13%	81%	—	2%	—	—	4%	—

[1]Surface unidentified.
[2]Surface weld-line.
[3]Surface crack.
[4]Surface nodule.
[5]Surface blister.
[6]Internal unidentified.
[7]Internal spherical pore.
[8]Internal non-spherical porosity.

bundle strength by 50% to 100%. The Young's modulus was unaffected by heat treatment, and the average modulus measured from all the tests (based on the slope of the stress-strain response) was 355 ± 25 GPa. This was slightly less than the modulus reported for Nextel™ 610 single filaments (380 GPa) [13].

4.1. Fractography

The defect population in the filaments after failure of the bundle was determined from SEM micrographs. The results are listed in Table II and compared well to the observations from the single filament tests [10]. Similar to the single filament tests, 50% of the failures in the as-received condition were due to internal defects. As the exposure temperature increased, the observation of internal defects decreased, and the observation of weld-line defects (a remnant of filament-to-filament sintering) increased. After exposure at 1450°C, over 80% of the failures were due to weldline defects.

Although the defect populations were similar in the single filament and bundle tests, the position of the weld-line defect on the fracture surface was different. The weld-line defects from single filament tests were shown to be slightly offset from the focal point of the fracture mirror [10]. In contrast, the weld-line defects from the bundle tests were at the focal point in over 90% of the filaments (see Fig. 4a). A tendency for the crack to initiate and grow at an angle to the plane perpendicular to the tensile axis also was apparent (see Fig. 4b). This indicates that the stress state around the "weld" or bond line was different in the two tests.

Filament clusters consisting of two, three, and four filaments were observed after failure; a four filament cluster is shown in Fig. 5. If filament failure was independent of neighboring filaments, the probability that a filament would fail within a diameter of its neighbor is equal to the filament diameter (12 μm) divided by the gauge length (2.54 cm) or $\sim 5 \times 10^{-4}$. Similarly, the probability of three filaments failing within a filament diameter is $\sim 2.5 \times 10^{-7}$, and for four filaments, $\sim 10^{-10}$. Therefore, the observations of filaments clusters imply that bonded filaments are not independent. The bonded filaments will transfer load from a broken filament directly to neighboring filaments. Therefore, the global load sharing assumption will not be valid for filaments clusters, and the cluster will likely fail when the weakest filament within the cluster fails.

4.2. Filament cluster characterization

To characterize the extent of clustering, the distribution of clusters was measured from polished cross sections of sintered bundles. The multifilament clusters were counted from SEM micrographs. The number of single filaments was then determined by subtracting the total number of filaments in clusters from the average number of filaments in a bundle (396). The average cluster distribution from three cross sections at each temperature is shown in Table III. As the exposure temperature increased, the number of filaments in clusters increased.

The fractography results indicated over 80% of the filaments failed from weld-line defects after exposure to 1450°C whereas only 35% would be expected from the 2-D cluster distribution measurements. This discrepancy indicates the filaments were not bonded over their entire length. This was confirmed by direct observation of a diminishing filament-to-filament bond (see Fig. 6).

5. Non-ideal bundle modeling

The non-ideal bundle modeling described in the following sections is based on a generalized bundle

TABLE III Filament cluster distribution: Average number of clusters per exposure temperature

Exposure temperature	Cluster size											
	1	2	3	4	5	6	7	8	10	13	14	18
As-received	383	5	1									
1300°C	368	9	2	1								
1400°C	309	17	7	3	1	1	0.3	0.3			0.3	
1450°C	254	16	11	2	3	2	1	1	0.3	0.3	1	0.3

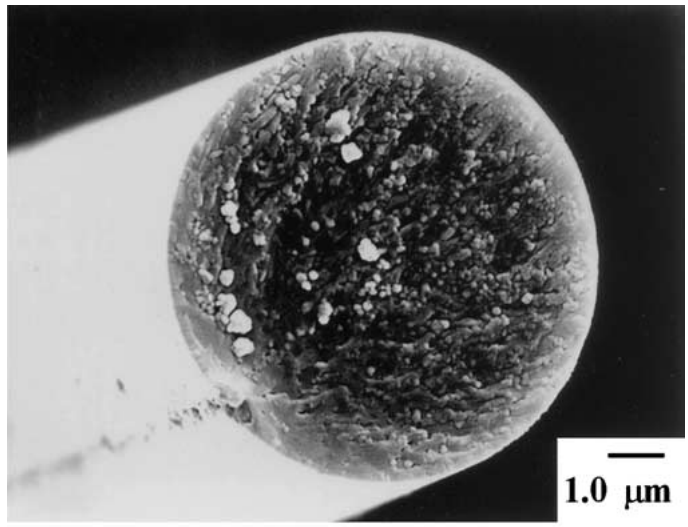

(a)

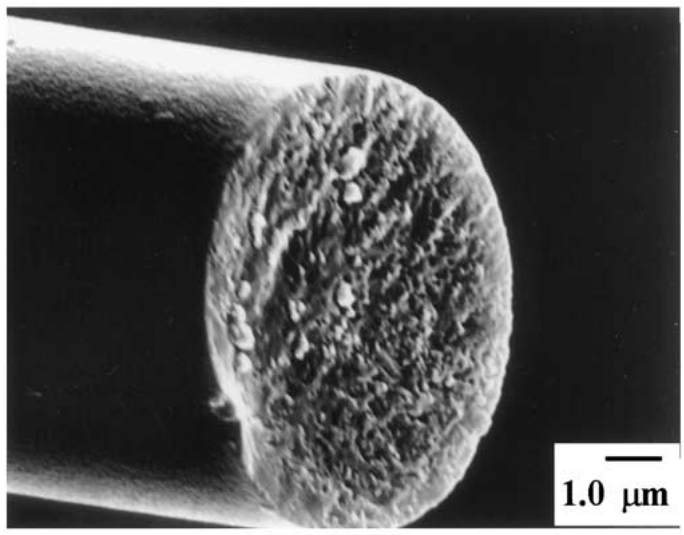

(b)

Figure 4 Example of a fracture surface from a bundle test. (a) Failure initiated at a weld-line defect: defect at focal point of fracture mirror, (b) Crack propagation was often observed to initially begin at an angle to the expected direction for pure mode I failure.

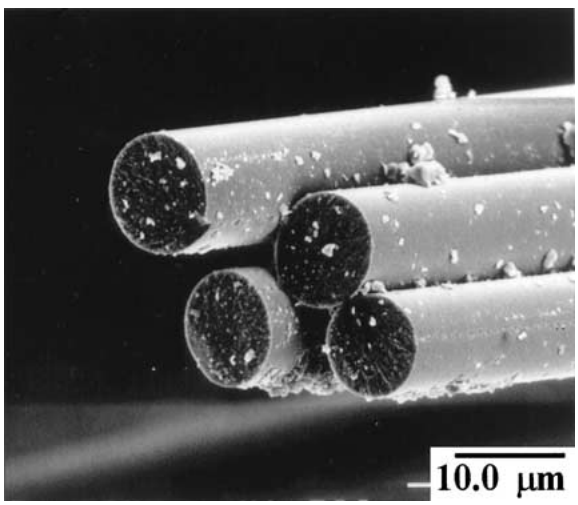

Figure 5 Failure of filament cluster in a bundle exposed at 1450°C; filament failure occurs on or near the same plane.

model developed by Phoenix [14] and Monte Carlo simulations. Three bundle defects are modelled: filament slack, filament misalignment and filament clusters.

5.1. Filament slack

Filament slack results from variations in filament length over a given bundle gauge length. Length variations in the Nextel™ 610 fiber tow are apparent in Fig. 1. During the straining of a bundle, shorter filaments will be loaded first followed by the longer filaments. This creates a bundle whose filaments have a distribution of strains.[2]

Phoenix [14] developed a generalized bundle model to consider a bundle with a distribution of strains. The Phoenix approach was to calculate the expected value of the bundle stress for a certain filament type, i, and then sum over the different types; filaments with different elastic moduli would be considered different filament types. The bundle stress is then:

$$\sigma_b = \sum_i^n V_i \int_0^{\varepsilon_b} E_{fi}\, \varepsilon (1 - P_{fi}(\varepsilon)) g(\varepsilon)\, \mathrm{d}\varepsilon \qquad (6)$$

[2] In a composite where the matrix resists relative filament motion, variations in filament length will be manifested as a filament-misalignment defect rather than a filament-slack defect.

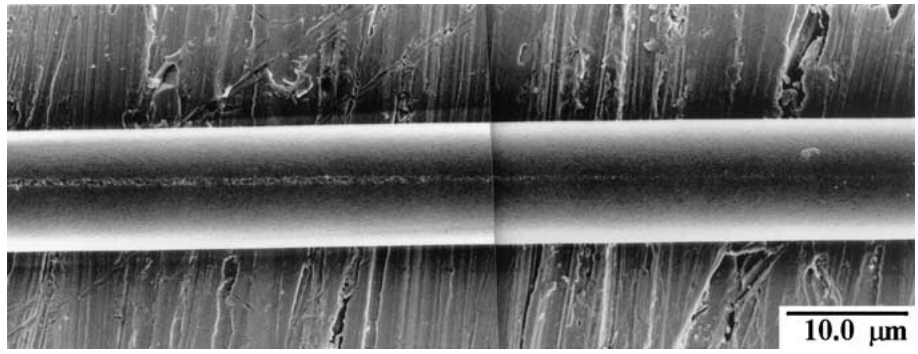

Figure 6 Weld-line defect on a filament removed from a bundle exposed at 1450°C. The width and depth of the weld-line defect decrease from left to right indicating the filament was not bonded over its entire length.

where n is the total number of filament types; ε_b is the maximum strain in the bundle (i.e. the strain of a perfectly aligned filament); $P_{fi}(\varepsilon)$ is the probability of failure, and $g(\varepsilon)$ is the probability density function describing the distribution of strains. The integral term is the expected value for the bundle stress of the filament type, i.

To consider the effect of filament slack on the bundle stress, a filament-slack parameter, Θ, is defined for each filament, j, of type, i:

$$\Theta = \frac{l_j - l_o}{l_o} \tag{7}$$

where l_j is the total length of an individual filament and l_o is the initial length of the bundle. Θ is the bundle strain at which filament j begins to carry load. Therefore, $\varepsilon_b - \Theta$ is the strain of an individual filament. Assuming that a filament carries no load when $\varepsilon_b - \Theta < 0$ and is perfectly aligned when $\varepsilon_b - \Theta > 0$, Equation 6 can be rewritten as:

$$\sigma_b = \int_o^{\Theta_{\max}} E_f(\varepsilon_b - \Theta) \times \exp\left(-\frac{L}{L_o}\left(\frac{E_f(\varepsilon_b - \Theta)}{\sigma_o}\right)^m\right) g(\Theta)\,\mathrm{d}\Theta \tag{8}$$

substituting the Weibull function for the probability of failure and recognizing that there is only one filament type in Nextel^{TM} 610. $\Theta_{\max}$ is the maximum value of the filament-slack parameter. Equation 8 is the expected value of the bundle stress given a distribution in the filament-slack parameter, $g(\Theta)$.

One reasonable distribution function for the filament-slack parameter is a linear decreasing function such as:

$$g(\Theta) = -\frac{2}{\Theta_{\max}^2}\Theta + \frac{2}{\Theta_{\max}}, 0 < \Theta < \Theta_{\max} \tag{9}$$

This type of distribution represents the realistic case where most of the filaments have very little slack.

For $\varepsilon_b > \Theta_{\max}$, the bundle stress can be calculated from Equation 8 while for $\varepsilon_b < \Theta_{\max}$, the expected bundle stress becomes:

$$\sigma_b = \int_o^{\varepsilon_b} E_f(\varepsilon_b - \Theta) \times \exp\left(-\frac{L}{L_o}\left(\frac{E_f(\varepsilon_b - \Theta)}{\sigma_o}\right)^m\right) g(\Theta)\,\mathrm{d}\Theta \tag{10}$$

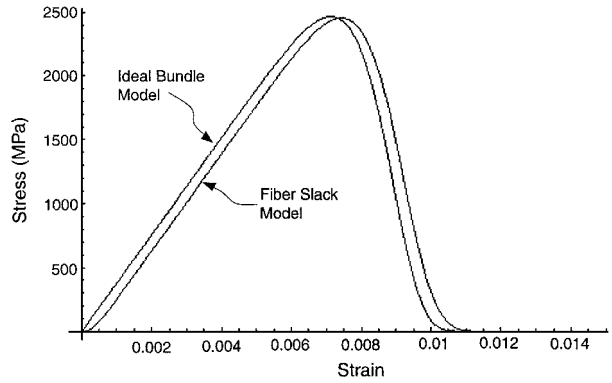

Figure 7 Stress-Strain response of an ideal bundle compared to one with filament slack; the Weibull parameters used were from the as-received single filaments [10].

The stress-strain response of an ideal bundle compared to one with a maximum filament-slack parameter of 0.001 is shown in Fig. 7.[3] The filament-slack model predicted that the initial Young's modulus is significantly less then an ideal bundle. As more filaments become loaded the stiffness increases until all the filaments are loaded and the stiffness response parallels the ideal bundle model. This type of response does not match the measured response, which was linear throughout and consistently 90% of the filament modulus. Filament-slack effects, therefore, can be ignored in this well aligned Nextel^{TM} 610 tow.

5.2. Filament misalignment

Misalignment is another mechanism that can cause a distribution in filament strains and decrease the modulus and strength. If it is assumed that the filament angle, ϕ_i, does not significantly change as the bundle is strained, then the axial strain in a misaligned filament is:

$$\varepsilon_i = \varepsilon_b \cos^2 \phi_i \tag{11}$$

Again using Phoenix's model, the bundle stress for a given ε_b becomes:

$$\sigma_b = \int_o^{\phi_{\max}} E_f\,\varepsilon_b \cos^2\phi_i \times \exp\left(-\frac{L}{L_o}\left(\frac{E_f\,\varepsilon_b \cos^2\phi_i}{\sigma_o}\right)^m\right) g(\phi_i)\,\mathrm{d}\phi_i \tag{12}$$

[3] The integral was numerically evaluated in *Mathematica*^{TM}.

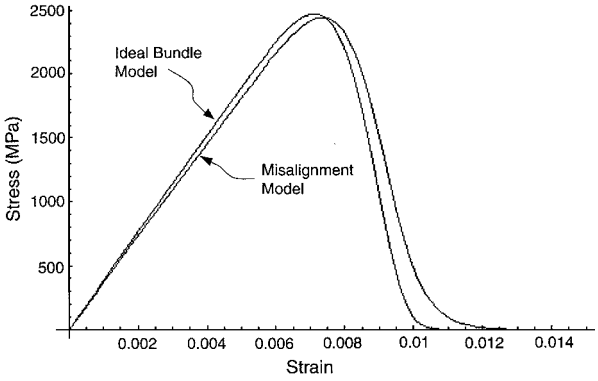

Figure 8 Stress-Strain response of a bundle with filament misalignment ($\phi_{max} = 30^\circ$) compared to the ideal bundle model.

Similar to the filament-slack model, the distribution of misalignment angles, $g(\phi_i)$, can be modeled as decreasing linearly from the angle zero to a maximum angle, ϕ_{max}. The stress-strain response of an as-received Nextel^{TM} 610 bundle with a maximum misalignment of 30° is plotted in Fig. 8 along with the ideal bundle prediction. The predicted modulus for this misalignment distribution is 360 GPa, which compares well to the measured bundle modulus. Also, unlike the filament slack mechanism, misalignment causes a consistent percentage decrease over the entire linear elastic region. However, this distribution of misalignment angles is not realistic. Warren [15] measured the misalignment angles between metal coated Nextel^{TM} 610 filaments prior to consolidation and determined that ϕ_{max} was no more than 6°. Using Warren's misalignment distribution, the predicted Young's modulus was 378 GPa. Therefore, misalignment in Nextel^{TM} 610 will only contribute a part of the loss in modulus. It will be shown later that misalignment will affect the ultimate bundle strength when filaments are bonded together.

5.3. Filament clusters

Both the generalized Phoenix bundle model and Monte Carlo simulations were used to model the effects of bonded filament clusters. The assumptions were that the filaments were perfectly aligned (a reasonable assumption given the modeling results in the previous sections), a filament cluster failed at the failure stress of the weakest filament within that cluster, and the filament strength distribution was described by the measured Weibull parameters from the single filament tests. Therefore the probability of failure for a cluster type i can be written as:

$$P_{fi} = 1 - \exp\left(-\frac{C_i L}{L_o}\left(\frac{E_{fi}\varepsilon}{\sigma_o}\right)^m\right) \qquad (13)$$

where C_i is the number of filaments in cluster type i. The term C_i essentially increases the volume of the filament, effectively increasing the probability of failure. Substituting Equation 13 into Equation 6 and assuming the filaments are perfectly aligned (i.e. $g(\varepsilon_b) = 1$), the filament-cluster bundle stress is:

$$\sigma_b = \sum_i^n V_i E_f \varepsilon \exp\left(-\frac{C_i L}{L_o}\left(\frac{E_f \varepsilon}{\sigma_o}\right)^m\right) \qquad (14)$$

Similar to the ideal bundle model, the bundle strength is defined as:

$$\sigma_b^* = \sum_i^n V_i \sigma_{fail} c_i^{-1/m} \exp\left(-\frac{1}{m}\right) \qquad (15)$$

As a first approximation, volume fraction of each cluster type was assumed to be equivalent to the measured values in Table III. The response of the cluster model was compared to the ideal bundle model and measurements in Fig. 2. The cluster model indicates that the ultimate bundle strength is lowered as clustering increases but does not fully explain the large drop in measured strength after heat treatments at 1400°C and 1450°C.

Monte Carlo simulations of bundle tests were also performed to verify the accuracy of the Phoenix approach. The same assumptions were considered. To assign strengths to the 396 filaments in a bundle, a random number between 0 and 1 was generated. This number was taken to be the failure probability, P_f. Substituting this P_f into Weibull function, the strength of that filament was calculated and assigned. The strength of the clusters was determined by assigning a strength to each filament within the cluster, finding the lowest filament strength, and then assigning this lowest strength to all the filaments within the cluster.

With these assumptions and rules for assigning filament strengths, the bundle stress-strain response was simulated using *Mathematica*^{TM}. For each cluster characterization in Table III, two simulations were performed. The results in Fig. 9 for as-received Nextel^{TM} 610 show very good agreement between the Phoenix model and the Monte Carlo simulations; similar results were found for the exposed bundles. However, neither model captures the large decreases in strength measured for the heat treatment at 1400°C and 1450°C.

As discussed earlier, the fractography indicated more filament-to-filament sintering than did the two-dimensional measurements of clusters. In particular for the bundles exposed to 1450°C, 80% of the filaments failed due to a weld-line defects (i.e. 80% were in clusters) compared to the two-dimensional observations that 35% of the filaments were in clusters. This discrepancy was modeled using the Monte Carlo method by assuming that 80% of the filaments were in one

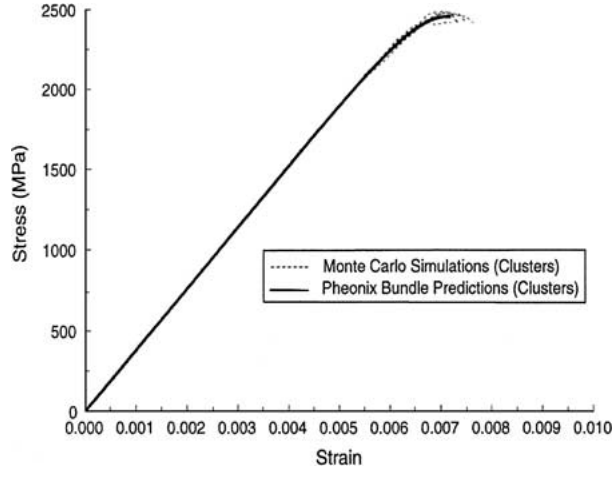

Figure 9 Monte Carlo simulations compared to cluster modeling using the Phoenix approach for as-received Nextel^{TM} 610.

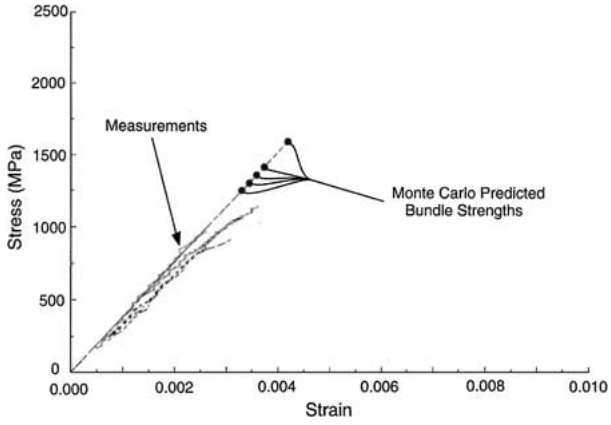

Figure 10 Stress-Strain response of bundles exposed at 1450°C with the Monte Carlo prediction of the worst case scenario (i.e. the bundle fails when the weakest filament fails).

cluster. With a cluster this large, the bundle essentially failed when the weakest filament failed, which may be considered a worst case scenario. The results of five simulations are shown in Fig. 10; the simulations still overpredicts the measured bundle strength.

6. Discussion

The evidence of filament clusters failing on essentially the same plane (Fig. 5) clearly indicates that filament failure was dependent on neighboring filaments. In other words, the global load sharing assumption is invalid for filament clusters. However, the filament cluster model, which assumed the filament strengths were characterized by the single filament tests and the filament clusters failed when the weakest filament failed, did not fully explain the differences between theory and experiment. One must conclude then that the single filaments removed from filament clusters have a higher strength than while they are still bonded together, and therefore, do not accurately describe the strength distribution of the bonded filaments.

An important difference between the single filament and bundle tests concerns the timing of when the filaments are torn from the clusters. In the single filament tests, the filaments were removed before testing so the roughness of the weld-line defects were created before failure. The sintering stresses were also relieved. In contrast, the filaments remained bonded during the bundle testing, and the roughness of the weld-line defect was created after testing; either from the shock waves associated with failure or by manually removing the filaments.

The central issue is the single filament tests are measuring the strength distribution of defects created by removing bonded filaments from the bundle. In one sense, the weld-line defects are not actually present in the bundles because they are created after failure. This would seem to indicate that there was a difference in the defect distribution, and therefore, it seems obvious that the strength distribution from the single filament tests would not accurately describe the strength distribution of filaments still bonded together. However in Part I [10], it was found that grain boundary grooves either created by separation of bonded filaments or from thermal etching likely controlled strength. Given that grain boundary grooves from thermal etching were present in the bonded filaments, the differences in the strength of bonded filaments and single filaments with weld-line defects are likely not due to differences in the defect population.

A consideration of the fracture surfaces will give some insight into why the bonded filaments in bundles have a lower strength then when removed from those bundles. In the single filament tests, the weld-line defects were shown to be offset from the focal point of the fracture mirror. In contrast, the bonded filaments in bundle tests exhibited different fracture features. First, in over 90% of the filaments the weld-line defect was at the focal point of the fracture mirror. Second, in approximately 50% of the bundle filaments, which failed from a weld-line defect, the initial crack growth occurred at an angle to the normal of the applied stress (Fig. 4). These differences indicated that the stress state around the weld-line was significantly different in the bonded and unbonded cases.

One potential reason for the different stress state is that the sintering stresses associated with the neck were relieved when creating the weld-line defect. The stress state normal to the neck area has been investigated by a number of researchers [16, 17]. Zhang and Schneibel [17] showed that tensile stresses on the order of 100 MPa are present at the neck surface; a result of capillary pressure. These stresses decrease moving inward and ultimately change to compression. To the author's knowledge, the stress state parallel to the axis of sintered filaments has not been determined. The bonded filaments are under plain strain condition along this axis, and therefore some induced axial stresses are expected. However, since the sintering stress is very localized, it seems unlikely they would have a significant effect on filament strength.

Another factor that may cause the stress to increase in bonded filaments is the constraint of relative filament motion. As can be seen in Fig. 1, the filaments will not be perfectly aligned and under a tensile load will likely move relative to one another. In Fig. 11 the

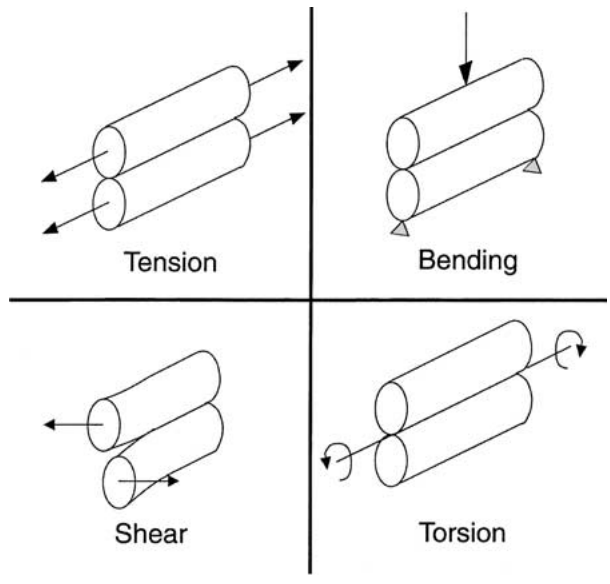

Figure 11 Schematic representation of a sintered filament pair, and the types of deformation that may occur during tensile testing.

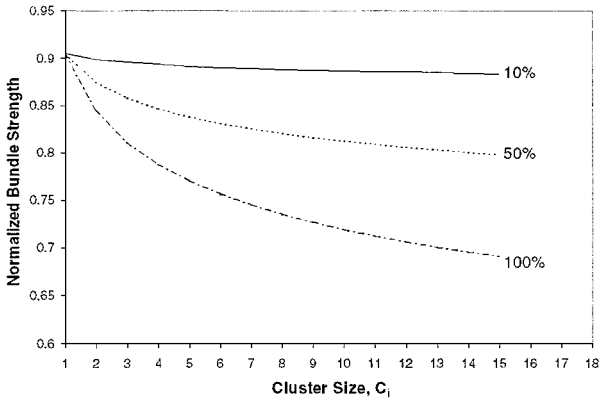

Figure 12 Normalized bundle strength ($\sigma_b^*/\sigma_{\text{fail}}$) plotted versus cluster size for bundles with 10%, 50% and 100% clusters. Bundles assumed to consist of individual filaments and clusters of size, C_i.

four different types of deformation of bonded filaments are schematically drawn. Finite element analysis was used to examine how the application of tensile, bending, shear and torsion stresses affects the stress state around the weld-line [18]. The model geometry was based on a single filament pair with a single weld-line. The results showed that the stress around the weld-line was not enhanced in simple tension. Shear deformation induced stresses around the transition from bonded to unbonded filaments, but these stresses were induced in such a small volume that this type of deformation is not likely important. However, in bending and torsion of bonded filament pairs, shear stresses are induced down the entire length of the weld-line [18].

The presence of the induced shear stresses around the weld-line indicates that mixed-mode failure may be occurring in the filaments that remain bonded. These induced stresses and a potential mixed-mode failure would effectively decrease the filament strength compared to the single filament tests, which helps explain the mispredictions of the bundle strength after heat treating at 1400°C and 1450°C. However, the degradation of filament strength requires that the filaments remain bonded together during the relative motion. Since, the bundle strength was well predicted for exposures at or below 1300°C (Fig. 3), the filament bonds were likely broken by the relative motion of the filaments during testing. For exposures at or above 1400°C, the filament bonds must be strong enough to resist fracture from relative motion.

In a composite where relative filament motion is inhibited by the matrix material, one would expect the induced stresses around the weld-line to be insignificant. The non-ideal cluster model (Section 5.3), which assumes the strength distribution from the single filament tests,[4] is the appropriate bundle model used in conjuction with unidirectional composite strength models [1, 2] when filament-to-filament sintering occurs. In the case where the reinforcements are woven, the effect of the misalignment must be considered. For a unidirectional reinforced composite, the effect of filament clustering can be estimated by plotting the bundle strength in Equation 15 normalized to σ_{fail} as a function of cluster size, C_i (see Fig. 12). If 10% of the filaments within a bundle are in clusters, the bundle strength is not significantly affected. If 100% of the filaments were in fifteen-filament clusters, the bundle strength would only decrease approximately 23%. This analysis assumes global load sharing behavior between clusters. If the clusters remain independent from neighboring filaments, 10% clustering within a composite can be tolerated.

[4] The single filaments tests did appear to describe the strength distribution of Nextel^{TM} 610 in a porous alumina matrix composite [18].

7. Conclusions

The strength of the Nextel^{TM} 610 alumina tow decreased as the exposure temperature increased. The bundles behaved ideally when the amount of filament-to-filament sintering was limited, and the filament bonds fractured from relative filament motion during testing. In addition, it was determined that filament slack and filament misalignment were not significant defects in the Nextel^{TM} 610 tow. When the filaments did remain bonded during testing, the ideal bundle model overpredicted the failure stress and strain. Two reasons for this discrepancy were identified. First, filaments within bonded clusters are no longer independent of their neighbors and will likely fail when the weakest filament within the cluster fails. Second, bonded filaments will fail at a lower than expected stress when compared to the strength of unbonded filaments.

The lower strength of the bonded filaments was due to a stress intensification around the weld-line, which resulted from bending or torsion of the bonded filaments. Specifically, shear stresses were induced causing fracture to possibly occur via a mixed mode in the bonded filaments rather than only mode I as in the unbonded filaments. Fractography showing an initial off-axis crack propagation corresponds to this view of failure.

The effect of filament-to-filament sintering within a composite should be less severe than in a "dry" bundle since the matrix material will limit relative motion of the filaments. Without the bending or torsion of bonded filament pairs, there should be no induced stress at the bond line, i.e., no decrease in the measured reference stress from the single filament tests. In addition, a composite may be more sensitive to the lower temperature sintering since relative filament motion can not break the bonds between the lightly sintered filaments. Therefore, the non-ideal cluster model (Section 5.3) is the appropriate bundle model to be used in conjunction with composite strength models when filament-to-filament sintering occurs. Assuming global load sharing behavior between the clusters, the model indicates that 10% clustering within a composite can be tolerated.

Acknowledgements

The author is grateful to H. N. G. Wadley for serving as dissertation advisor for this work. The author also appreciates the many helpful discussions with D. Elzey, C. Herakovich and D. Wilson and practical assistance with the experimental work from P. Schare, T. Eanes and W. Shoupe. This work was supported by an AFOSR-URI grant #F49620-93-1-0359.

References

1. B. W. ROSEN, *AIAA Journal* **2**(11) (1964) 1985.
2. W. A. CURTIN, *J. Amer. Ceram. Soc*. **74**(11) (1991) 2837.
3. F. T. PIERCE, *J. Text. Inst*. **17T** (1926) 355.
4. M. M. PLATT, *Text. Res. J*. **20**(1) (1950) 1.
5. H. E. DANIELS, *Proc. Royal Soc. Lond*. **183A** (1945) 405.
6. B. D. COLEMAN, *J. Mech. Phys. Solids* **7** (1958) 60.
7. R. R. KIESCHKE, H. E. DEVE, C. MCMULLOUGH and C. J. GRIFFIN, in "Recent Advances in Titanium Metal Matrix Composites," edited by F. H. Froes and J. Storer (TMS Publication, 1995) p. 3.
8. P. CANTONWINE and H. DEVE, in "Recent Advances in Titanium Metal Matrix Composites," edited by F. H. Froes and J. Storer (TMS Publication, 1995) p. 201.
9. C. G. LEVI, J. Y. YANG, B. J. DALGLEISH, F. W. ZOK and A. G. EVANS, *J. Amer. Ceram. Soc*. **81**(8) (1998) 2077.
10. P. CANTONWINE, *J. Mater. Sci.* **38** (2003) 461.
11. S. PHOENIX and R. RAJ, *Acta Metall. Mater*. **40**(10) (1992) 2813.
12. M. M. VOGEL-MARTIN and D. M. WILSON, in Proceedings from the 16th Conference on Metal Matrix, Carbon and Ceramic Matrix Composites; NASA conference publication 3175 part 2 (1992) p. 519.
13. D. M. WILSON, personal communication.
14. S. L. PHOENIX, *Fibre Science and Technology* **7** (1974) 15.
15. J. M. WARREN, Ph.D. Dissertation, University of Virginia, 1994.
16. H. E. EXNER and P. BROSS, *Acta Metall*. **27** (1979) 1007.
17. W. ZHANG and J. H. SCHNEIBEL, *J. Amer. Ceram. Soc*. **79**(8) (1996) 2141.
18. P. E. CANTONWINE, Ph.D. Dissertation, University of Virginia, August 1999.

Received 11 March
and accepted 24 September 2002